BULLETIN OF THE POLISH ACADEMY OF SCIENCES
TECHNICAL SCIENCES, Vol. 72(6), 2024, Article number: e151044
DOI: 10.24425/bpasts.2024.151044



# Experimental investigations of ultra-lightweight-concrete encased cold-formed steel structures: local stability behavior of C-section profiles subjected to eccentric compression

**Ahmed ALABEDI*** **and Péter HEGYI**

Department of Structural Engineering, Budapest University of Technology and Economics, Hungary

**Abstract.** Nowadays, cold-formed steel (CFS) has become widely used in the field of lightweight structures. In 2016, the Budapest University of Technology and Economics initiated a research study on a unique structural system using CFS and utilized ultra-lightweight concrete as an encasing material. This material serves as continuous bracing that improves CFS element resistance, stability behavior and performance, while also manifesting heat insulation capabilities, thus helping achieve sustainability goals. This paper is considered a continuation of previous research conducted by the authors. An experimental investigation was carried out on encased CFS columns subjected to eccentric loading. A total of fourteen stub-columns, with two distinct thicknesses, were subjected to various loading conditions for testing. The test results showed that local failure controlled the behavior of all the tested elements. The reduction in capacity resulting from eccentricity with respect to centric resistance varied between 20% and 52%, depending on the load position applied and on the core thickness of the tested steel elements. Moreover, the test outcomes were compared to the Eurocode analytical solution of pure steel elements. The overall load increment ranged from 46% to 18%, with a more noticeable bracing impact observed in the case of slender elements. Material tests also supplement the results.

**Keywords:** cold-formed steel; experimental test; lightweight concrete; continuous bracing; sustainability.

## 1. INTRODUCTION

In modern constructions, cold-formed steel (CFS) structure systems have become increasingly used as alternates for common building materials such as hot-rolled steel and reinforced concrete. The advantageous properties of this material, including its ease of fabrication, rapid assembly and lightweight nature, have played a pivotal role in popularizing such structures [1]. As load-bearing element, CFS exhibits failure modes related to stability, such as local, distortional or global buckling and interaction. The boundary conditions in a building, such as a bracing system or sheathing, strongly influence the stability of CFS frames and the resulting failure modes. As the influence is positive, new specifications should incorporate these effects in design procedures to improve the performance of structural systems, to help reduce the material needs and to create a more sustainable environment. This has drawn the attention of numerous researchers who seek to solve these issues. In the literature, many researchers have investigated the CFS bracing effect, which can be broken down into two distinct groups: (i) discrete connections, exemplified by sheathing, and (ii) continuous bracing, which incorporates infill materials [2]. The concept of discrete bracing was investigated by Telue *et al.* [3, 4], with the performance of a CFS wall lined with plasterboard being deeply analyzed to provide design recommendations based on the Australian design code. These guidelines consider an effective length based on the space between the screws. Similarly, Schafer *et al.* [5–8] conducted extensive research and theoretical analysis investigating sheathing bracing. Their work aimed to provide design criteria that could account for the different behaviors of sheathed CFS, improving the AISI specifications. Moreover, the performance of sheathed CFS walls remained the main topic for a long time; numerous researchers have conducted various experiments and numerical investigations covering various types of sheathing materials, including gypsum, calcium silicate, oriented-strand, and reinforced cement board considering different load conditions, such as axial, seismic design, monotonic shear, dynamic, cyclic lateral and cyclic shear [9–14].

Conversely, many researchers have extensively investigated the concept of continuous bracing. Here the main idea is to incorporate the stabilizing effect of a continuous lightweight material which initially only serves as a heat insulator. This can result in a double win situation for sustainability: the heat insulation reduces the load bearing material usage, too. It also encourages the use of specific heat insulation materials. In [15, 16], the performance of composite CFS walls was tested under axial compressive loads using lightweight flue gas desulfurization gypsum and phosphogypsum (PG) as infill material. The experimental framework results demonstrated that incorporating such lightweight fillers can significantly enhance the axial compressive strength of CFS walls. Xu *et al.* [17–19] examined the high-strength lightweight foamed concrete (HLFC) effect on the

*e-mail: alabedi.ahmed@edu.bme.hu

Manuscript submitted 2024-03-13, revised 2024-05-29, initially accepted for publication 2024-06-19, published in November 2024.

performance of cold-formed steel (CFS) shear walls. The consequences demonstrated that adding infill significantly improves the seismic performance of the tested specimens and shifts the resulting failure mode from brittle to ductile. Likewise, Wang and colleagues [20–22] undertook experimental investigations of composite CFS shear walls, utilizing several types of filler materials, including lightweight polymer material (LPM) [20, 21] and light EPS mortars (LEM) [22]. Their findings highlighted the significant influence of these infill materials on the load-bearing capacity, seismic performance and energy dissipation on all tested specimens.

In [23, 24], another enhancement was implemented by continuously braced corrugated steel sheets with various foamed concretes. The findings demonstrated substantial influence of the infill material, as the lightweight foamed concrete enhanced the structural response, creating a novel structural system with sufficient load-carrying capability suitable for application in low-rise residential constructions. Eltayeb *et al.* [25, 26] thoroughly investigated the profile double-skin steel composite wall (PSCW) filled with foam and rubberized foam concrete (FRC). Researchers used various rubber content to examine PSCW behavior under axial compressive forces [25] and eccentric compressions [26]. Their research aimed to provide a comprehensive analysis of the structural performance of FRC-filled PSCWs, and their findings indicated that FRC can be effectively utilized as an infill material, giving adequate capacities appropriate for residential building constructions.

Apart from infills, in practical applications, CFS sections often experience both bending moment and compressive load simultaneously due to loading eccentricity at connection points between walls and floors or walls and roofs. In structural engineering, it is essential to understand the performance of such an element. Thus, many researchers have addressed the problem and investigated it. In [27], a novel built-up CFS section was carefully investigated under eccentric compressive load by conducting thirty-three experimental tests to analyze buckling behavior and interaction effects between compression and bending. Their findings showed that existing design standards generally underestimate the strength of these members. Thirty-three experimental tests revealed that current design standards often underestimate their strength. Similarly, Ziqi *et al.* [28] numerically analyzed built-up CFS channels with V-stiffeners and Σ-stiffeners under different loading conditions, finding conservative estimates in both Chinese and North American design standards, and proposing a new interaction equation. Likewise, a series of investigations were conducted on lipped C-profile to evaluate and improve existing design code predictions in [29, 30]. Peiris *et al.* [29] revealed that current design guidelines underestimate load-bearing capacities using 35-lipped channel column tests and finite element analyses. Czechowski *et al.* [30] investigated the effects of load eccentricities on lipped C-profiles, revealing significant reductions in maximum load as compared to axially loaded columns. Considerable experimental and numerical studies in this field have explored lipped CFS columns, considering diverse eccentricities and different thicknesses [31, 32].

In 2016, the Budapest University of Technology and Economics, Department of Structural Engineering, started an extensive research program on polystyrene aggregate concrete (PAC) encased CFS sections. As a filling material, PAC can provide heat, moisture insulation and fire protection, owing to its polystyrene granules and admixtures composition instead of gravel or sand [33]. In [1, 34–36], PAC was introduced as a promising and efficient construction material that can be used beneficially in residential buildings. The experimental results indicated that PAC-bracing markedly restrained global buckling failure, improving the stability of centrally loaded CFS columns and flexural strength of tested specimens, resulting in load-bearing capacity enhancements of 10–110% and 30–190%, respectively. Moreover, the PAC-braced CFS test sections were numerically assessed [37], the behavior was deeply investigated, and a Eurocode-based design method was presented [2, 38]. In addition to providing thermal insulation, the observations indicate that the PAC encasing material significantly enhances the load-bearing capacity of cold-formed steel (CFS). These improvements render PAC an ideal multifunctional construction material. Consequently, the development and application of the proposed design method helps achieve sustainability goals.

## 2. STRUCTURAL DESCRIPTION AND GOALS

To help understand the build-up of the structural system under investigation, the skeleton of a selected part of a building can be seen in Fig. 1. As in the case of light-gauge construction, the load bearing elements of both wall and slab are the steel ribs made up of CFS C-sections. These C-sections are connected by U-tracks at both ends of the panels, the steel formwork is then encased in PAC. Panels are connected at their ends by special connectors which can transfer specific types of load components. Due to the nature of the connections, the load transmission cannot be fully centric, thus even the internal wall ribs are subjected to eccentric axial force, which emphasizes the necessity of investigating this behavior. Previous research indicated that the most important failure mode is local buckling, thus the experimental investigations were carried out on small, separated pieces of the wall, i.e. stub-columns having limited length.

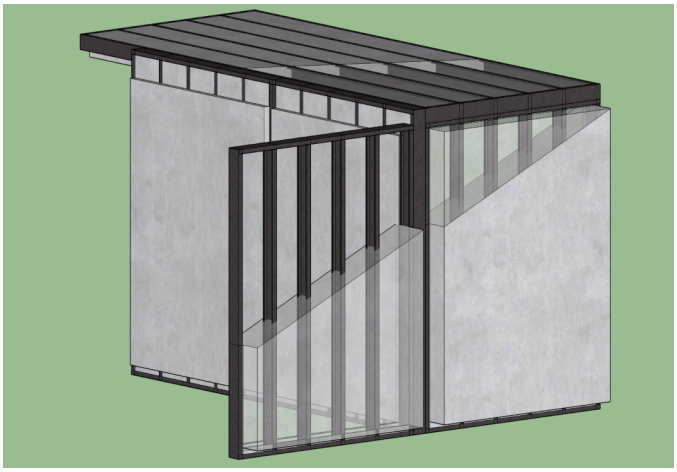

**Fig. 1.** Novel building system

The aim of the current paper is to expand the available experimental results already published in [1, 2, 34–36, 38] to include a new loading type, i.e. eccentric compression. The behavior, load bearing capacity and effect of different cross-sections will be discussed herein, which is necessary to make further developments to the proposed design method in [2].

## 3. EXPERIMENTAL WORK

### 3.1. Test specimens

Altogether, fourteen encased specimens were investigated in the presented experiments, applying two different steel cross-section thicknesses. Comprehensive investigation was conducted on C-section column elements having 150 mm in web height, made of S350GD grade galvanized with a zinc coat of Z275. The column length was 300 mm. The same joint configuration described in [35] was used with a 300 mm long U-section of 150 mm in height fastened at both ends of the C-section column with one self-drilling screw through the flanges of the sections, creating a column-end joint and a stable loading surface. To further strengthen the connection, 50 × 50 mm angle sections of 2 mm in thickness were attached to the web of the U and C-sections, ensuring that the failure would occur within the column rather than in the connection zone. Two self-drilling screws were used to establish the connection between the web of the tested C-profile and the angle section. In contrast, spot welding was used to create the link between the upper U-section web and the angle.

All tested elements were embedded in a 300 mm × 300 mm polystyrene aggregate concrete block of the same mixture. Moreover, Table 1 along with Fig. 2 and 3 illustrate all the dimensions, configurations and nomenclature of specimens used within this study.

**Table 1**
CFS sections dimensions

| # | Section | Nominal thickness [mm] | H [mm] | B1 [mm] | B2 [mm] | C [mm] |
|---|---|---|---|---|---|---|
| 1 | C150 | 1 | 150 | 42 | 48 | 14.4 |
| 2 | C150 | 2 | 150 | 42 | 48 | 18.4 |
| 3 | U150 | 1 | 150 | 50 | 50 | – |

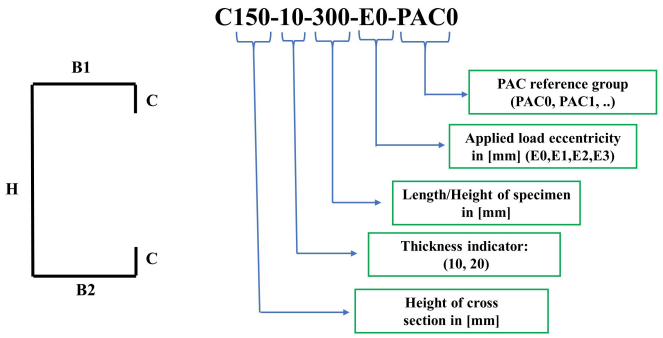


**Fig. 2.** Nomenclature of specimens

### 3.2. Material properties

In addition to conducting tests on structural members, comprehensive material testing was undertaken to demonstrate the PAC mechanical properties accurately. By definition, PAC is a concrete mixture containing cement and polystyrene granules, with some admixtures to improve material workability and properties [33]. As gravel is absent from the mixture, the mechanical properties of the PAC closely resemble those of foams, mainly controlled by the quantity of cement paste [2]. Hence, due to the cement segregation phenomenon, high scatter in PAC properties

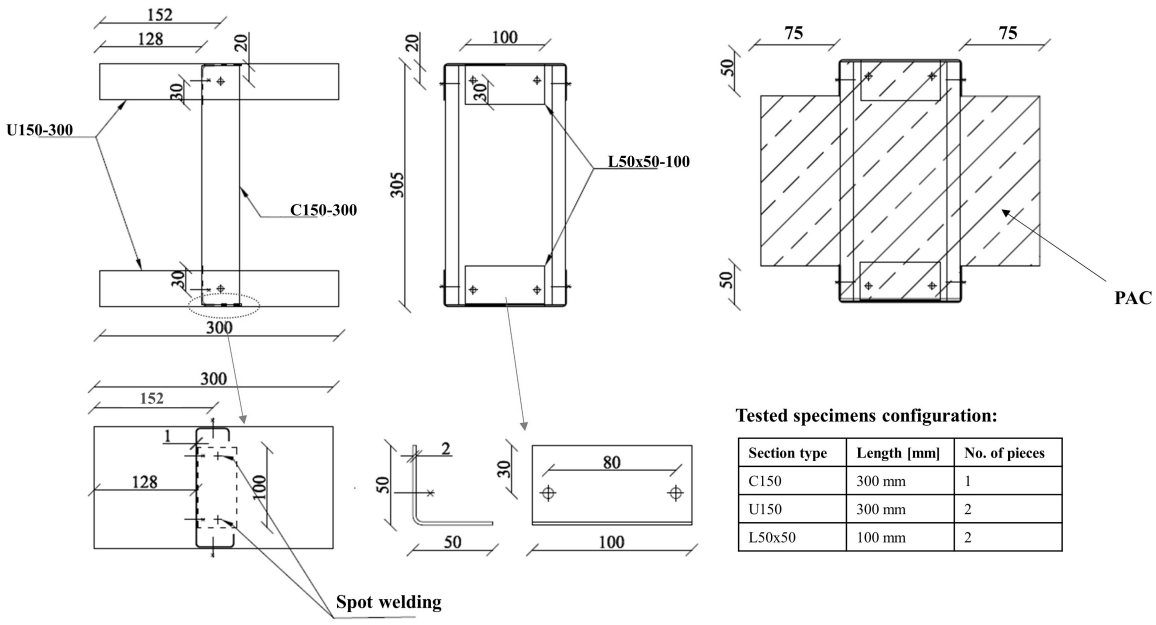


**Fig. 3.** Tested C-section details

can be achieved even within one type of mixture. For practical use, the material characteristics can be assessed by the bulk density of the mixture, which is directly correlated with the amount of cement present [34, 35].

In the tests, one mixture type was used. The tested material specimens were divided into six groups to track PAC properties and avoid high segregation by reducing concrete pouring time. Comprehensive assessments were conducted on eighteen 150 mm cubes and 70 mm × 70 mm × 250 mm prisms to determine PAC material compressive and flexural strengths and Young's modulus for all six groups. Analogously to the structural specimens, the PAC specimens were maintained in a controlled laboratory environment and tested at 28 days of age.

The test results were found to be consistent with those previously reported in [1, 34] (see Fig. 4). For more accuracy, the density of PAC is directly calculated in CFS specimens to ensure that material tests share the same properties as the structural specimens, see Table 2. The table data illustrates a good correlation between the bulk density of the material and the structural specimens, revealing the reliability of material measurements. The data measured will later become the basis for a finite element sensitivity analysis to identify the effect of the material properties on the load bearing capacity.

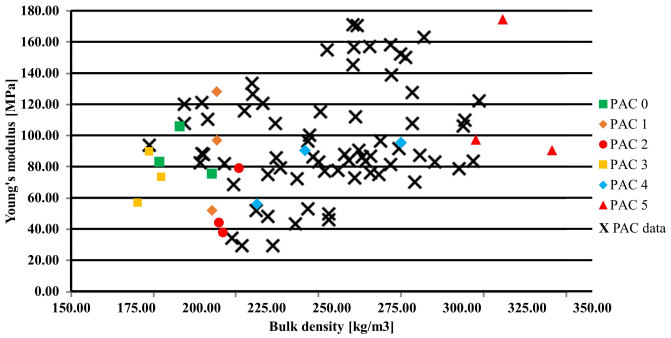


**Fig. 4.** PAC Young's modulus vs literature data

Moreover, Fig. 5 illustrates the influence of the amount of cement paste on the compressive strength of PAC, as shown by the correlation between concrete cube test results and density; notably, denser PAC mixtures tend to exhibit higher compressive strengths. In conclusion, the PAC data were deemed reliable and lay within the expected range. Steel properties were assessed through a series of twelve coupon tests for two different thicknesses, as detailed in Table 3.

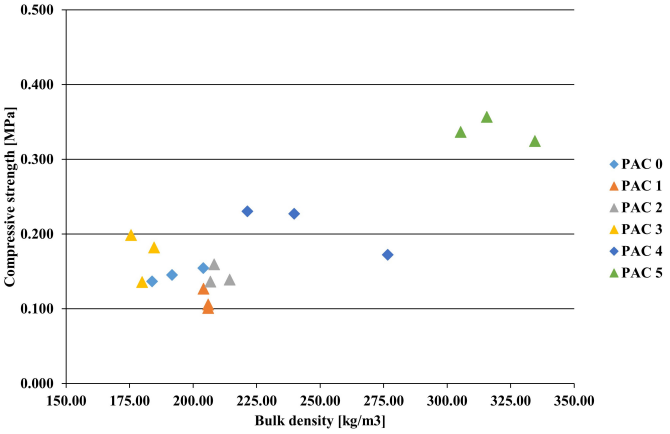


**Fig. 5.** PAC compressive strength vs bulk density

**Table 3**
Results of coupon tests

| # | Nominal thickness [mm] | Yield strength [N/mm$^2$] | Tensile strength [N/mm$^2$] |
|---|---|---|---|
| 0 | 1.0 | 322 | 397 |
| 0 | 2.0 | 405 | 546 |
| 1 | 1.0 | 370 | 470 |
| 2 | 2.0 | 429 | 487 |

**Table 2**
Results of material tests for PAC

| Denotation of mixture | Bulk density*1 [kg/m$^3$] | Bulk density*2 [kg/m$^3$] | Compression strength [N/mm$^2$] | Flexural strength [N/mm$^2$] | Young's modulus [kN/mm$^2$] | Corresponding structural specimens |
|---|---|---|---|---|---|---|
| PAC0 | 193 | 214 | 0.147 | 0.151 | 100.14 | C150-10-300-E0<br>C150-20-300-E0 |
| PAC1 | 247 | 238 | 0.111 | 0.24 | 92.31 | C150-10-300-E1 |
| PAC2 | 203 | 200 | 0.145 | 0.14 | 53.60 | C150-10-300-E2 |
| PAC3 | 186 | 223 | 0.172 | 0.11 | 73.32 | C150-10-300-E3<br>C150-20-300-E2 |
| PAC4 | 235 | 224 | 0.210 | 0.17 | 80.57 | C150-20-300-E1 |
| PAC5 | 308 | 341 | 0.339 | 0.30 | 120.74 | C150-20-300-E2 |

*1 Bulk density measurement of material test

*2 Bulk density measurement of structural specimens

### 3.3. Test setup

A 480 mm long hot rolled load-transferring frame of 20 mm in thickness was attached to both ends of the column using self-drilling screws to ensure the transfer of eccentric loading to the C-section (see Fig. 6). The loading process was conducted with a Zwick Z400 universal testing machine in the age of 28 days of PAC. The load applied was precisely directed onto the outer surface of the load-transferring frame at varying eccentricities measured from the center of gravity of gross cross-section of the C-profile in accordance with Table 4. One-directional eccentricities were applied to induce a bending moment over the strong axis. A constant rate of displacement-controlled loading was maintained throughout the test. Axial displacement was monitored through four sensor transducers, as illustrated in Fig. 6. After each test, the CFS-braced specimen was disassembled to examine the steel core failure mode.

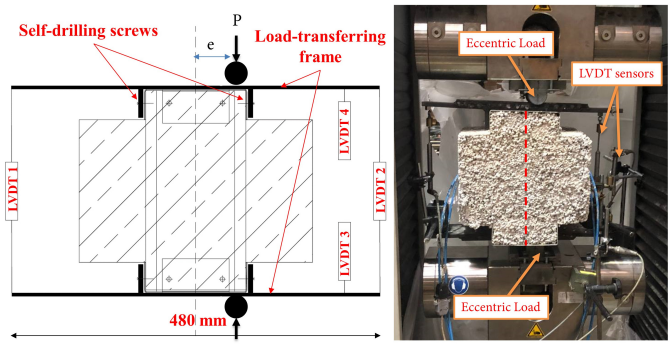


**Fig. 6.** Zwick Z400 universal machine and sensor locations

**Table 4**
Experimental data

| # | Eccentricity being considered | Notation | Yield strength [N/mm$^2$] | Number of specimens |
|---|---|---|---|---|
| C150-10-300 | 0 | E0 | 322 | 3 |
| C150-20-300 | 0 | E0 | 405 | 3 |
| C150-10-300 | h/4 | E1 | 370 | 2 |
| | h/3 | E2 | | 2 |
| | h/2 | E3 | | 1 |
| C150-20-300 | h/4 | E1 | 429 | 1 |
| | h/3 | E2 | | 2 |

## 4. TEST RESULTS

The experimental results revealed that local phenomena controlled the failure of all tested CFS specimens, marked by sudden failure comparable to those reported in [34]. The centrically loaded members produced local failure in the interior part of the specimen, close to the stiffened zone at the end joint. The web, flanges and stiffeners together suffered plate buckling, as illustrated in Fig. 7a. In the case of the eccentrically loaded specimens, failure shifted toward the flange having larger compression stress, indicating complex interaction between the axial and bending effects (see Fig. 7b). Table 5 shows the test results of the 1 mm thick specimen. Compared to the centrally loaded specimens, the total reduction in load-carrying capacity from the induced bending moment varied between 30% and 52%.

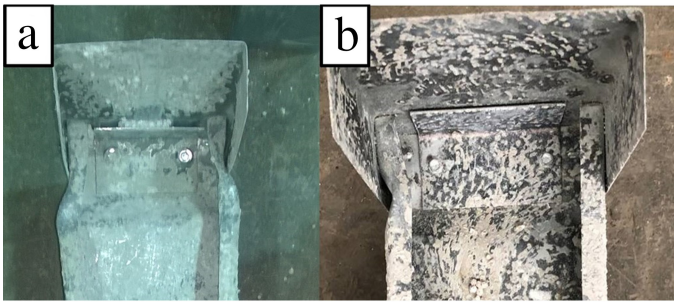


**Fig. 7.** (a) Failure mode of centrically loaded specimen, (b) failure mode of eccentrically loaded specimen

**Table 5**
Results of 1 mm specimens

| # | Ultimate capacity [kN] | Average capacity [kN] | Unbraced analytical solution [kN] | Increment [%] |
|---|---|---|---|---|
| C150-10-300-E0 | 43.94 | 42.03 | 28.75 | 46.00 |
| | 43.36 | | | |
| | 38.80 | | | |
| C150-10-300-E1 | 33.60 | 33.66 | 24.19 | 39.00 |
| | 33.73 | | | |
| C150-10-300-E2 | 28.38 | 28.88 | 22.47 | 28.00 |
| | 29.38 | | | |
| C150-10-300-E3 | 22.94 | 22.94 | 19.68 | 17.00 |

To demonstrate the PAC-bracing effect, the results of the encased CFS specimens were compared to the standardized resistance of the unbraced steel section following the Eurocode procedure, considering the shift of centroid due to elastic plate buckling. An increment of 46% resulted from encasing PAC in the centrically loaded specimen (i.e. E0), revealing PAC's substantial impact on the CFS element's stability and consenting with those stated in [34]. Other eccentricities resulted in lower load increments of 39%, 28%, and 17% for (E1), (E2), and (E3), respectively. Such a reduction in loading capacity is expected due to the interaction buckling phenomenon caused by induced bending. The different applied eccentricities induced additional stresses on the C-flange, leading to failure at a lower axial force. However, it is evident that the effectiveness of PAC was also impacted by the application of bending moment, as it could not maintain consistent enhancement levels. This can be attributed to the stress gradient in the web, which results

in shorter buckling widths and a higher number of buckling sine waves over shorter lengths. Consequently, when buckling lengths are reduced, stiffness of the steel becomes more dominant over PAC-stiffness (i.e. higher k$\sigma$ buckling factor), thus it has a more significant influence over the overall behavior [2].

With three distinct load cases, the results of the 2 mm thick specimen were also compared to the analytical solution to investigate the core steel thickness effect. Similarly, Table 6 demonstrates the experimental results of PAC-braced specimens. For centrically loaded specimens, a lower load increment of 18% resulted from encasing material, revealing that the PAC is more effective in the case of more slender elements than thicker ones. According to the design equations in [2] and given that the two tested groups share the same material properties (PAC0), with a smaller b/t = 75 ratio, the critical buckling of steel is higher, causing the stiffness of the steel to be more dominant than the encasing material, resulting in lower effectiveness of PAC.

**Table 6**
Results of 2 mm specimens

| # | Ultimate capacity [kN] | Average capacity [kN] | Unbraced analytical solution [kN] | Increment [%] |
|---|---|---|---|---|
| C150-20-300-E0 | 125.00 | 130.27 | 110.48 | 18.00 |
| | 140.00 | | | |
| | 125.82 | | | |
| C150-20-300-E1 | 109.74 | 109.74 | 80.55 | 36.00 |
| C150-20-300-E2 | 81.90 | 86.50 | 73.24 | 18.00 |
| | 91.10 | | | |

However, the influence of PAC was found to be more effective in other load cases. It can be seen that (h/4) eccentricity (refer to C150-20-300-E1) resulted in a higher load increment of 36%, which is quite close to the 1 mm specimen (refer to C150-10-300-E1). Nevertheless, the load increment was found to be lower in the case of (h/3) eccentricity with 1 mm thickness indicating a nonlinearity in behavior and complex impact of steel core thickness. Hence, different encasing materials stiffness and steel core thicknesses need to be assessed. This nonlinearity in behavior requires deep examination, and the range of study needs to be extended using both numerical and analytical tools.

On the other hand, Fig. 8 demonstrates the load-displacement curves of all tested CFS specimen types. It can be noticed that all tested elements exhibit different initial stiffness for different load cases and core steel thickness; a continuous change in stiffness could be seen due to increasing the load. Figure 9 displays the C150-20-300-E1 load-displacement data, which can be separated into three phases. Initially, up to ~ 5 mm, there is a progressive increase in stiffness, which can be attributed to the closing of the initial gap between the C-section and the U, with tolerance in screws location. Subsequently, up to the maximum load, displacement increases, showing an almost constant stiffness, influenced by the core steel's stiffness. Following the failure phase, where the C-section experiences a loss in stiffness, displacement undergoes a rapid escalation. As the Young's modulus of the PAC is significantly smaller than that of steel, normal stiffness of the bracing material is also distinctly smaller, thus it does not play an important role in the data measured.

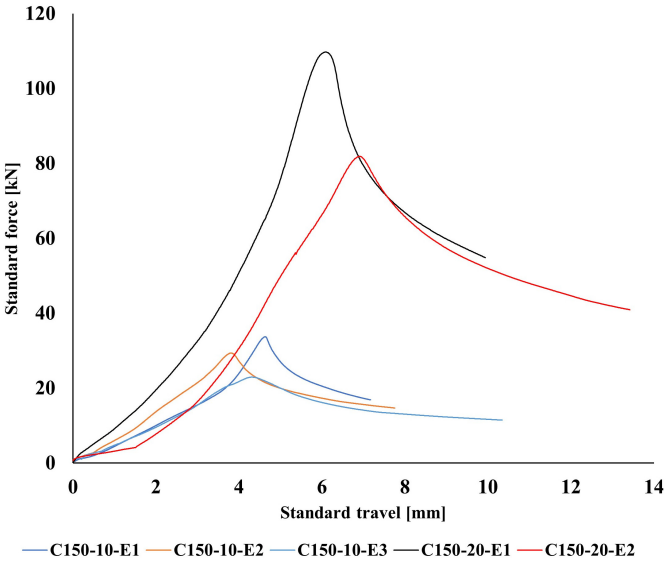


**Fig. 8.** Load-displacement curves for different eccentricities being considered

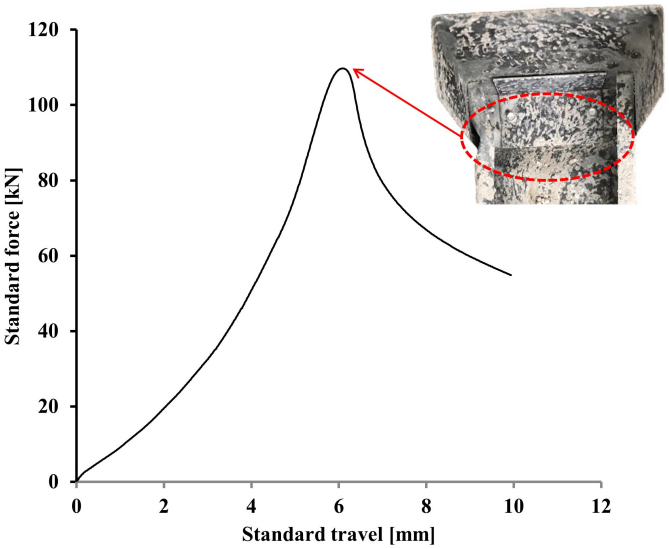


**Fig. 9.** Test data for C150-20-300-E1 (load-displacement curve)

Finally, Fig. 10 demonstrates the end joint outward rotation curves for the C150-20-300-E1, in which LVDT 1 and LVDT 2 are the total approach and separation between the top and the bottom flanges (measurements were filtered from the axial deformations to show the rotations only). In contrast, LVDT 3 and LVDT 4 display the bottom and top end rotation, respectively. It is evident that LVDT 1 and LVDT 2 show identical behavior,

whereas LVDT 4 shows a higher degree of rotation than LVDT 3 due to its proximity to the failure zone. Table 7 presents rotation data at failure for all tested specimens for the top and bottom edges, with their corresponding bending moments. It can be observed that results are rather scattered, which can be the consequence of different reasons. The PAC material properties were scattered, and the initial gap between C and U elements of the specimens were not the same. The sensor transducers used provided more detailed data for the structural behavior under an eccentric load that can be utilized later for FEM analyses.

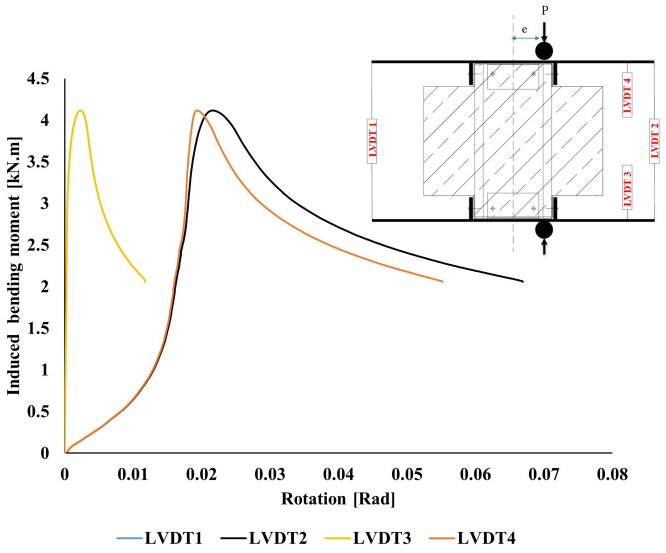


**Fig. 10.** Test data for C150-20-300-E1 end joint rotation

**Table 7**
Top and bottom column edges rotation

| # | Maximum moment [kNm] | Top edge rotation [mrad] | Bottom edge rotation [mrad] |
|---|---|---|---|
| C150-10-300-E1 | 1.26 | 23.6 | 9.1 |
| | | 10.1 | 8.5 |
| C150-10-300-E2 | 1.44 | 16.7 | 5.1 |
| | | 18.6 | 7.1 |
| C150-10-300-E3 | 1.72 | 22.1 | 19.1 |
| C150-20-300-E1 | 4.12 | 19.4 | 2.3 |
| C150-20-300-E2 | 4.32 | 38.7 | 11.2 |
| | | 7.9 | 10.5 |

## 5. CONCLUSION

This paper introduces an experimental research program conducted at the Budapest University of Technology and Economics, Department of Structural Engineering, focusing on the local behavior of cold-formed steel (CFS) elements encased in polystyrene aggregate concrete (PAC) under eccentric axial loads. A comprehensive set of fourteen PAC-braced CFS specimens underwent testing, allowing to arrive at the following fundamental conclusions:

1. Local failure phenomena near the stiffened zone dominated the behavior of all tested specimens.
2. The reduction in load-carrying capacity due to the bending moment being induced ranged between 20% and 52%, depending on load location and core steel thickness.
3. Compared to the unbraced steel standardized resistance, the total load increment ranged from 46% to 18%, demonstrating the substantial impact of polystyrene aggregate concrete on the stability of the CFS element.
4. The bracing effect of polystyrene aggregate concrete was more evident in the case of slender specimens than thicker ones.
5. The test results demonstrated that the effectiveness of PAC decreased due to stress gradients in the web, leading the steel stiffness to be more dominant and significantly influencing overall behavior.
6. Besides assessing the load-carrying capacity, PAC mechanical properties were also evaluated by performing concrete prism and cube tests, ensuring a thorough understanding of the material's behavior.
7. The measured material properties are in the range of previous results; the bulk density measurements on structural specimens demonstrated a good correlation between the material and structural specimen tests.
8. The sensor transducer results showed notable scatter due to PAC material properties and contrast in the initial gap between the C and U elements.

Despite the advances made to date, the field needs further numerical and analytical investigations to better understand these complex interactions and refine the original design and analysis approaches in order to help build a more sustainable future.

## ACKNOWLEDGEMENTS

The reported R&D project is funded by the Government of Hungary by means of "Funding to SMEs and large companies for RDI activities" (2018-1.1.2-KFI-2018-00150). The Stipendium Hungaricum Scholarship founding by the Hungarian Government, Tempus Public Foundation is thankfully acknowledged.

## REFERENCES

[1] P. Hegyi and L. Dunai, "Experimental study on ultra-lightweight-concrete encased cold-formed steel structures Part I: Stability behaviour of elements subjected to bending," *Thin-Walled Struct.*, vol. 101, pp. 75–84, Apr. 2016, doi: 10.1016/j.tws.2016.01.004.

[2] A. Alabedi and P. Hegyi, "Development of a Eurocode-based design method for local and distortional buckling for cold-formed C-sections encased in ultra-lightweight concrete under compression," *Thin-Walled Struct.*, vol. 196, p. 111504, Mar. 2024, doi: 10.1016/j.tws.2023.111504.

[3] Y. Telue and M. Mahendran, "Behaviour of cold-formed steel wall frames lined with plasterboard," *J. Constr. Steel Res.*, vol.

57, no. 4, pp. 435–452, Apr. 2001, doi: 10.1016/S0143-974X(00)00024-9.

[4] Y. Telue and M. Mahendran, "Behaviour and design of cold-formed steel wall frames lined with plasterboard on both sides," *Eng. Struct.*, vol. 26, no. 5, pp. 567–579, Apr. 2004, doi: 10.1016/j.engstruct.2003.12.003.

[5] B.W. Schafer, "Review: The Direct Strength Method of cold-formed steel member design," *J. Constr. Steel Res.*, vol. 64, no. 7–8, pp. 766–778, Jul. 2008, doi: 10.1016/j.jcsr.2008.01.022.

[6] L.C.M. Vieira Jr and B.W. Schafer, "Behavior and design of axially compressed sheathed wall studs," in *2010 – 20th International Specialty Conference On Cold-Formed Steel Structures*, 2010.

[7] L.C.M. Vieira, Y. Shifferaw, and B.W. Schafer, "Experiments on sheathed cold-formed steel studs in compression," *J. Constr. Steel Res.*, vol. 67, no. 10, pp. 1554–1566, Oct. 2011, doi: 10.1016/j.jcsr.2011.03.029.

[8] Kara D. Peterman, *Experiments on the stability of sheathed cold-formed steel studs under axial load and bending*, Johns Hopkins University, 2012.

[9] Y.S. Tian, J. Wang, and T.J. Lu, "Axial load capacity of cold-formed steel wall stud with sheathing," *Thin-Walled Struct.*, vol. 45, no. 5, pp. 537–551, May 2007, doi: 10.1016/j.tws.2007.02.017.

[10] L. Fiorino, O. Iuorio, and R. Landolfo, "Sheathed cold-formed steel housing: a seismic design procedure," *Thin-Walled Struct.*, vol. 47, no. 8–9, pp. 919–930, 2009, doi: 10.1016/j.tws.2009.02.004.

[11] C.-L. Pan and M.-Y. Shan, "Monotonic shear tests of cold-formed steel wall frames with sheathing," *Thin-Walled Struct.*, vol. 49, no. 2, pp. 363–370, Feb. 2011, doi: 10.1016/j.tws.2010.10.004.

[12] I. Shamim and C.A. Rogers, "Steel sheathed/CFS framed shear walls under dynamic loading: Numerical modelling and calibration," *Thin-Walled Struct.*, vol. 71, pp. 57–71, Oct. 2013, doi: 10.1016/j.tws.2013.05.007.

[13] W. Mowrtage (V. Karakale), "Cyclic lateral load behavior of CFS walls sheathed with different materials," *Thin-Walled Struct.*, vol. 96, pp. 328–336, Nov. 2015, doi: 10.1016/j.tws.2015.08.025.

[14] M. Accorti, N. Baldassino, R. Zandonini, F. Scavazza, and C.A. Rogers, "Reprint of Response of CFS Sheathed Shear Walls," *Structures*, vol. 8, pp. 318–330, Nov. 2016, doi: 10.1016/j.istruc.2016.07.002.

[15] H. Wu, S. Chao, T. Zhou, and Y. Liu, "Cold-formed steel framing walls with infilled lightweight FGD gypsum Part II: Axial compression tests," *Thin-Walled Struct.*, vol. 132, pp. 771–782, Nov. 2018, doi: 10.1016/j.tws.2018.06.034.

[16] C. Yin, L. Zhou, Q. Zou, and Y. Xu, "Effect of Filling Phosphogypsum on the Axial Compression Behavior of Cold-Formed Thin-Walled Steel Walls," *Buildings*, vol. 12, no. 9, p. 1325, Aug. 2022, doi: 10.3390/buildings12091325.

[17] Z. Xu, Z. Chen, B.H. Osman, and S. Yang, "Seismic performance of high-strength lightweight foamed concrete-filled cold-formed steel shear walls," *J. Constr. Steel Res.*, vol. 143, pp. 148–161, Apr. 2018, doi: 10.1016/j.jcsr.2017.12.027.

[18] Z. Xu, Z. Chen, and S. Yang, "Effect of a new type of high-strength lightweight foamed concrete on seismic performance of cold-formed steel shear walls," *Constr. Build. Mater.*, vol. 181, pp. 287–300, Aug. 2018, doi: 10.1016/j.conbuildmat.2018.06.067.

[19] Z. Xu, Z. Chen, and S. Yang, "Seismic behavior of cold-formed steel high-strength foamed concrete shear walls with straw boards," *Thin-Walled Struct.*, vol. 124, pp. 350–365, Mar. 2018, doi: 10.1016/j.tws.2017.12.032.

[20] W. Wang, J. Wang, T.Y. Yang, L. Guo, and H. Song, "Experimental testing and analytical modeling of CFS shear walls filled with LPM," *Structures*, vol. 27, pp. 917–933, Oct. 2020, doi: 10.1016/j.istruc.2020.06.016.

[21] W. Wang, J. Wang, P. Zhao, L. Ja, and G. Pan, "Axial compressive experiments and structural behaviour estimation of CFS composite walls sprayed with LPM," *J. Build. Eng.*, vol. 30, p. 101305, Jul. 2020, doi: 10.1016/j.jobe.2020.101305.

[22] W. Wang, J. Wang, and L. Guo, "Mechanical behavior analysis of LEM-infilled cold-formed steel walls," *Sustain. Struct.*, vol. 2, no. 1, p. 000013, 2022, doi: 10.54113/j.sust.2022.000013.

[23] M.A. Othuman Mydin and Y.C. Wang, "Structural performance of lightweight steel-foamed concrete–steel composite walling system under compression," *Thin-Walled Struct.*, vol. 49, no. 1, pp. 66–76, Jan. 2011, doi: 10.1016/j.tws.2010.08.007.

[24] E.A. Flores-Johnson and Q.M. Li, "Structural behaviour of composite sandwich panels with plain and fibre-reinforced foamed concrete cores and corrugated steel faces," *Compos. Struct.*, vol. 94, no. 5, pp. 1555–1563, Apr. 2012, doi: 10.1016/j.compstruct.2011.12.017.

[25] E. Eltayeb *et al.*, "Structural performance of composite panels made of profiled steel skins and foam rubberised concrete under axial compressive loads," *Eng. Struct.*, vol. 211, p. 110448, May 2020, doi: 10.1016/j.engstruct.2020.110448.

[26] E. Eltayeb, X. Ma, Y. Zhuge, J. Xiao, and O. Youssf, "Composite walls Composed of profiled steel skin and foam rubberized concrete subjected to eccentric compressions," *J. Build. Eng.*, vol. 46, p. 103715, Apr. 2022, doi: 10.1016/j.jobe.2021.103715.

[27] Q.-Y. Li and B. Young, "Tests of cold-formed steel built-up open section members under eccentric compressive load," *J. Constr. Steel Res.*, vol. 184, p. 106775, Sep. 2021, doi: 10.1016/j.jcsr.2021.106775.

[28] Z. He, S. Peng, X. Zhou, Z. Li, G. Yang, and Z. Zhang, "Design recommendation of cold-formed steel built-up sections under concentric and eccentric compression," *J. Constr. Steel Res.*, vol. 212, p. 108255, Jan. 2024, doi: 10.1016/j.jcsr.2023.108255.

[29] M. Peiris and M. Mahendran, "Behaviour of cold-formed steel lipped channel sections subject to eccentric axial compression," *J. Constr. Steel Res.*, vol. 184, p. 106808, Sep. 2021, doi: 10.1016/j.jcsr.2021.106808.

[30] L. Czechowski, M. Kotełko, J. Jankowski, V. Ungureanu, and A. Sanduly, "Strength analysis of eccentrically loaded thin-walled steel lipped C-profile columns," *Arch. Civ. Eng.*, vol. 3, no. 3, 2023, doi: 10.24425/ace.2023.146082.

[31] Ł. Borkowski, J. Grudziecki, M. Kotełko, V. Ungureanu, and D. Dubina, "Ultimate and post-ultimate behaviour of thin-walled cold-formed steel open-section members under eccentric compression. Part II: Experimental study," *Thin-Walled Struct.*, vol. 171, p. 108802, Feb. 2022, doi: 10.1016/j.tws.2021.108802.

[32] F.L. Bodea, I. Both, L. Czechowski, J. Jankoswki, M. Kotełko, and V. Ungureanu, "The Influence of Eccentricity on the Behaviour of Thin-Walled Cold-Formed Steel Members with Open

Cross-Sections under Compression," *ce/papers*, vol. 5, no. 4, pp. 186–193, Sep. 2022, doi: 10.1002/cepa.1744.

[33] É. Lublóy *et al.*, "Thermal insulation capacity of concretes by expanded polystyrene aggregate," in *4th International FIB Congress*, 2014, pp. 750–751.

[34] P. Hegyi and L. Dunai, "Experimental investigations on ultra-lightweight-concrete encased cold-formed steel structures," *Thin-Walled Struct.*, vol. 101, pp. 100–108, Apr. 2016, doi: 10.1016/j.tws.2016.01.003.

[35] P. Hegyi and L. Dunai, "Experimental Investigation of Thin-walled Column-end Joints Encased in Ultra-lightweight Concrete," *Period. Polytech.-Civ. Eng.*, vol. 61, no. 4, pp. 951–957, May 2017, doi: 10.3311/PPci.10041.

[36] P. Hegyi, L. Horváth, L. Dunai, and A.A.M. Ghazi, "Experimental Investigation of Shear Effects in Ultra-Lightweight Concrete Encased CFS Structural Members," *ce/papers*, vol. 5, no. 4, pp. 143–150, 2022, doi: 10.1002/cepa.1739.

[37] A. Alabedi and P. Hegyi, "Assessing the Equivalent Spring Method for Modelling of Lightweight-concrete Encased Cold-formed Steel Elements in Compression," *Period. Polytech.-Civ. Eng.*, vol. 68, no. 1, pp. 305–313, Oct. 2023, doi: 10.3311/PPci.22803.

[38] P. Hegyi and L. Dunai, "07.18: Cold-formed C-sections encased in ultra-lightweight concrete: Development of a Eurocode-based design method," *ce/papers*, vol. 1, no. 2–3, pp. 1647–1656, Sep. 2017, doi: 10.1002/cepa.208.